HOKKAIDO UNIVERSITY

Title	Design and laboratory demonstration of an achromatic vector vortex coronagraph
Author(s)	Murakami, Naoshi; Hamaguchi, Shoki; Sakamoto, Moritsugu et al.
Citation	Optics Express, 21(6), 7400-7410 https://doi.org/10.1364/OE.21.007400
Issue Date	2013-03-25
Doc URL	https://hdl.handle.net/2115/52784
Rights	© 2013 Optical Society of America, Inc.
Type	journal article
File Information	oe-21-6-7400.pdf

Hokkaido University Collection of Scholarly and Academic Papers : HUSCAP

Design and laboratory demonstration of an achromatic vector vortex coronagraph

Naoshi Murakami,[1,*] **Shoki Hamaguchi,**[2] **Moritsugu Sakamoto,**[2] **Ryohei Fukumoto,**[2] **Akitoshi Ise,**[2,3] **Kazuhiko Oka,**[1] **Naoshi Baba,**[1] **and Motohide Tamura**[4]

[1]*Division of Applied Physics, Faculty of Engineering, Hokkaido University, Kita-13, Nishi-8, Kita-ku, Sapporo, Hokkaido 060-8628, Japan*
[2]*Division of Applied Physics, Graduate School of Engineering, Hokkaido University, Kita-13, Nishi-8, Kita-ku, Sapporo, Hokkaido 060-8628, Japan*
[3]*Now with Nikon Corporation, 201-9, Miizugahara, Kumagaya, Saitama 360-8559, Japan*
[4]*National Astronomical Observatory of Japan, 2-21-1 Osawa, Mitaka, Tokyo 181-8588, Japan*
[*]*nmurakami@eng.hokudai.ac.jp*

Abstract: A vector vortex coronagraph (VVC) is one of promising means for imaging extremely faint objects around bright stars such as exoplanets. We present a design of an achromatic VVC, in which an axially-symmetric half-wave plate (AHP) is placed between crossed polarization filters (circular polarizer and analyzer). The circular polarizer and the analyzer are both composed of a polarizer and a quarter-wave plate (QWP). We demonstrate, via Jones calculus and Fourier analysis, that the achromatic stellar elimination can theoretically be realized by optimal polarization filters, even when chromatic AHP and QWPs are used. We carried out laboratory demonstrations of the designed VVC using a photonic-crystal AHP. As a result, we observed achromatic coronagraphic performance, a light suppression level of 7×10^{-5}, over a wavelength from 543 nm to 633 nm.

© 2013 Optical Society of America

OCIS codes: (350.1260) Astronomical optics; (230.5298) Photonic crystals; (050.4865) Optical vortices; (350.4238) Nanophotonics and photonic crystals.

References and links

1. P. Kalas, J. R. Graham, E. Chiang, M. P. Fitzgerald, M. Clampin, E. S. Kite, K. Stapelfeldt, C. Marois, and J. Krist, "Optical images of an exosolar planet 25 light-years from Earth," Science **322**, 1345–1348 (2008).
2. C. Marois, B. Macintosh, T. Barman, B. Zuckerman, I. Song, J. Patience, D. Lafrenière, and R. Doyon, "Direct imaging of multiple planets orbiting the star HR 8799," Science **322**, 1348–1352 (2008).
3. C. Thalmann, J. Carson, M. Janson, M. Goto, M. McElwain, S. Egner, M. Feldt, J. Hashimoto, Y. Hayano, T. Henning, K. W. Hodapp, R. Kandori, H. Klahr, T. Kudo, N. Kusakabe, C. Mordasini, J. -I. Morino, H. Suto, R. Suzuki, and M. Tamura, "Discovery of the coldest imaged companion of a sun-like star," Astrophys. J. **707**, L123–L127 (2009).
4. A. -M. Lagrange, M. Bonnefoy, G. Chauvin, D. Apai, D. Ehrenreich, A. Boccaletti, D. Gratadour, D. Rouan, D. Mouillet, S. Lacour, and M. Kasper, "A giant planet imaged in the disk of the young star β Pictoris," Science, **329**, 57–59 (2010).
5. G. Foo, D. M. Palacios, and G. A. Swartzlander, Jr., "Optical vortex coronagraph," Opt. Lett. **30**, 3308–3310 (2005).
6. D. Mawet, P. Riaud, O. Absil, and J. Surdej, "Annular groove phase mask coronagraph," Astrophys. J. **633**, 1191–1200 (2005).

#175941 - $15.00 USD Received 11 Sep 2012; revised 28 Oct 2012; accepted 30 Oct 2012; published 18 Mar 2013
(C) 2013 OSA

7. D. Rouan, P. Riaud, A. Boccaletti, Y. Clénet, and A. Labeyrie "The four-quadrant phase-mask coronagraph. I. principle," Publ. Astron. Soc. Pac. **112**, 1479–1486 (2000).
8. N. Murakami, R. Uemura, N. Baba, J. Nishikawa, M. Tamura, N. Hashimoto, and L. Abe, "An eight-octant phase-mask coronagraph," Publ. Astron. Soc. Pac. **120**, 1112–1118 (2008).
9. A. Carlotti, G. Ricort, and C. Aime, "Phase mask coronagraphy using a Mach-Zehnder interferometer," Astron. Astrophys. **504**, 663–671 (2009).
10. C. Jenkins, "Optical vortex coronagraphs on ground-based telescopes," Mon. Not. R. Astron. Soc. **384**, 515–524 (2008).
11. J. H. Lee, G. Foo, E. G. Johnson, and G. A. Swartzlander, Jr., "Experimental verification of an optical vortex coronagraph," Phys. Rev. Lett. **97**, 053901 (2006).
12. E. Mari, G. Anzolin, F. Tamburini, M. Prasciolu, G. Umbriaco, A. Bianchini, C. Barbieri, and F. Romanato, "Fabrication and testing of $l = 2$ optical vortex phase masks for coronography," Opt. Express **18**, 2339–2344 (2010)
13. G. A. Swartzlander, Jr., E. L. Ford, R. S. Abdul-Malik, L. M. Close, M. A. Peters, D. M. Palacios, and D. W. Wilson, "Astronomical demonstration of an optical vortex coronagraph," Opt. Express **16**, 10200–10207 (2008).
14. S. Pancharatnam, "Generalized theory of interference, and its applications," Proc. Indian Acad. Sci. **A44**, 247–262 (1956).
15. M. V. Berry, "The adiabatic phase and Pancharatnam's phase for polarized light," J. Mod. Opt. **34**, 1401–1407 (1987).
16. G. Biener, A. Niv, V. Kleiner, and E. Hasman, "Formation of helical beams by use of Pancharatnam-Berry phase optical elements," Opt. Lett. **27**, 1875–1877 (2002).
17. A. Niv, G. Biener, V. Kleiner, and E. Hasman, "Formation of linearly polarized light with axial symmetry by use of space-variant subwavelength gratings," Opt. Lett. **28**, 510–512 (2003).
18. A. Niv, G. Biener, V. Kleiner, and E. Hasman, "Spiral phase elements obtained by use of discrete space-variant subwavelength gratings," Opt. Commun. **251**, 306–314 (2005).
19. G. Biener, Y. Gorodetski, A. Niv, V. Kleiner, and E. Hasman, "Manipulation of polarization-dependent multivortices with quasi-periodic subwavelength structures," Opt. Lett. **31**, 1594–1596 (2006).
20. A. Niv, G. Biener, V. Kleiner, and E. Hasman, "Manipulation of the Pancharatnam phase in vectorial vortices," Opt. Express **14**, 4208–4220 (2006).
21. A. Niv, G. Biener, V. Kleiner, and E. Hasman, "Polychromatic vectorial vortex formed by geometric phase elements," Opt. Lett. **32**, 847–849 (2007).
22. Y. Gorodetski, G. Biener, A. Niv, V. Kleiner, and E. Hasman, "Space-variant polarization manipulation for far-field polarimetry by use of subwavelength dielectric gratings," Opt. Lett. **30**, 2245–2247 (2005).
23. G. Biener, A. Niv, V. Kleiner, and E. Hasman, "Space-variant polarization scrambling for image encryption obtained with subwavelength gratings," Opt. Commun. **261**, 5–12 (2006).
24. D. Mawet, N. Murakami, C. Delacroix, E. Serabyn, O. Absil, N. Baba, J. Baudrand, A. Boccaletti, R. Burruss, R. Chipman, P. Forsberg, S. Habraken, S. Hamaguchi, C. Hanot, A. Ise, M. Karlsson, B. Kern, J. Krist, A. Kuhnert, M. Levine, K. Liewer, S. McClain, S. McEldowney, B. Mennesson, D. Moody, H. Murakami, A. Niessner, J. Nishikawa, N. O'Brien, K. Oka, P. Park, P. Piron, L. Pueyo, P. Riaud, M. Sakamoto, M. Tamura, J. Trauger, D. Shemo, J. Surdej, N. Tabirian, W. Traub, J. Wallace, and K Yokochi, "Taking the vector vortex coronagraph to the next level for ground- and space-based exoplanet imaging instruments: review of technology developments in the USA, Japan, and Europe," in *Techniques and Instrumentation for Detection of Exoplanets V*, S. Shaklan, ed., Proc. SPIE, **8151**, 815108 (2011).
25. C. Delacroix, P. Forsberg, M. Karlsson, D. Mawet, O. Absil, C. Hanot, J. Surdej, and S. Habraken, "Design, manufacturing, and performance analysis of mid-infrared achromatic half-wave plates with diamond subwavelength gratings," Appl. Opt. **51**, 5897–5902 (2012).
26. D. Mawet, E. Serabyn, K. Liewer, Ch. Hanot, S. McEldowney, D. Shemo, and N. O'Brien, "Optical vectorial vortex coronagraphs using liquid crystal polymers: theory, manufacturing and laboratory demonstration," Opt. Express **17**, 1902–1918 (2009).
27. D. Mawet, E. Serabyn, K. Liewer, R. Burruss, J. Hickey, and D. Shemo, "The vector vortex coronagraph: laboratory results and first light at Palomar Observatory," Astrophys. J. **709**, 53–57 (2010).
28. E. Serabyn, D. Mawet, and R. Burruss, "An image of an exoplanet separated by two diffraction beamwidths from a star," Nature (London) **464** 1018–1020 (2010)
29. G. A. Swartzlander, Jr., "Achromatic optical vortex lens," Opt. Lett. **31**, 2042–2044 (2006).
30. Y. Tokizane, K. Oka, and R. Morita, "Supercontinuum optical vortex pulse generation without spatial or topological-charge dispersion," Opt. Express **17**, 14517–14525 (2009).
31. N. Murakami, and N. Baba, "Pupil-remapping mirrors for a four-quadrant phase mask coronagraph," Publ. Astron. Soc. Pac. **117**, 295–299 (2005).
32. L. Abe, N. Murakami, J. Nishikawa, and M. Tamura, "Removal of central obscuration and spider arm effects with beam-shaping coronagraphy," Astron. Astrophys. **451**, 363–373 (2006).
33. D. Mawet, E. Serabyn, J. K. Wallace, and L. Pueyo, "Improved high-contrast imaging with on-axis telescopes using a multistage vortex coronagraph," Opt. Lett. **36**, 1506–1508 (2011).

#175941 - $15.00 USD Received 11 Sep 2012; revised 28 Oct 2012; accepted 30 Oct 2012; published 18 Mar 2013
(C) 2013 OSA

34. G. A. Swartzlander, Jr., "Broadband nulling of a vortex phase mask," Opt. Lett. **30**, 2876–2878 (2005).
35. N. Murakami, N. Baba, A. Ise, M. Sakamoto, and K. Oka, "Laboratory demonstration of an optical vortex mask coronagraph using photonic crystal," in *Proceedings of the conference In the Spirit of Lyot 2010: Direct Detection of Exoplanets and Circumstellar Disks*, A. Boccaletti, ed., (University of Paris Diderot, Paris, France, 2010).
36. S. Kawakami, T. Kawashima, and T. Sato, "Mechanism of shape formation of three-dimensional periodic nanostructures by bias sputtering," Appl. Phys. Lett. **74**, 463–465 (1999).
37. T. Kawashima, K. Miura, T. Sato, and S. Kawakami "Self-healing effects in the fabrication process of photonic crystals," Appl. Phys. Lett. **77**, 2613–2615 (2000).
38. N. Murakami, J. Nishikawa, K. Yokochi, M. Tamura, N. Baba, and L. Abe, "Achromatic eight-octant phase-mask coronagraph using photonic crystal," Astrophys. J. **714**, 772–777 (2010).

1. Introduction

In recent years, several giant exoplanets (planets orbiting around stars other than the Sun) have been directly imaged by utilizing high-contrast imaging techniques [1–4]. In the future, further innovative instruments would be required for strongly eliminating glaring star light to a level of 10^{-10} for directly imaging Earth-like exoplanets. An optical vortex coronagraph is a promising concept of the high-contrast instrument, because of its small inner working angle (an innermost angular separation from a central star where high-contrast imaging is feasible), high throughput, and large discovery space [5, 6]. The optical vortex coronagraph embeds a complex phase function $e^{-i\ell_p\theta}$ (ℓ_p is a topological charge and θ is an azimuth angle) in an image of a parent star. When a coronagraphic mask generates the optical vortex with the spiral phase of an even topological charge ($\ell_p = \pm 2, \pm 4, \cdots$), a bright star light can theoretically be removed with a Lyot stop and a faint planet can directly be imaged [6]. We note that other types of focal-plane coronagraphic masks, a four-quadrant [7], eight-octant [8], and 4*N*-segment [9] phase masks, are also promising because of their detection ability and simple mask design. Mathematically, these masks are expressed as weighted sum of optical vortex masks with various even topological charges [8–10].

Two types of vortex masks, scalar and vector vortex ones, have been proposed for the coronagraph. The scalar vortex mask is a spiral dielectric plate with a space-variant thickness as a function of the azimuth angle θ to manipulate a phase delay [5]. Coronagraphic scalar vortex masks have been manufactured not only for laboratory demonstrations [11, 12] but also on-sky observations [13]. The vector vortex mask, on the other hand, is a space-variant birefringent optical element (SVBOE) with an optic axis as a function of θ [6] for manipulating the Pancharatnam-Berry's phase [14, 15]. The SVBOE based on subwavelength gratings have been well studied [16–21], and developed for various applications [22, 23] as well as the coronagraphic purpose [24, 25]. Coronagraphic vector vortex masks made of liquid-crystal polymers have been manufactured not only for laboratory demonstrations [24, 26], but also on-sky observations [27, 28].

For detecting extremely faint exoplanets and characterizing them through spectroscopic measurements, it is necessary to design achromatic high-contrast instruments. An achromatic scalar vortex mask has been proposed using two dielectric materials [29]. In addition, it has been proposed that an achromatic vector vortex mask can be realized by an axially-symmetric half-wave plate (AHP), a half-wave plate with space-variant fast axes corresponding to the azimuth angle θ, placed between polarization filters (crossed circular polarizer and analyzer) [24, 26]. Both the circular polarizer and the analyzer are composed of a linear polarizer and a quarter-wave plate (QWP). We note that a similar optical system has been proposed for generating supercontinuum optical vortex pulse, where an axially-symmetric polarizer is used instead of the AHP [30].

In this paper, we demonstrate that a fully achromatic vector vortex mask is theoretically realized even when chromatic AHP and QWPs are used. In Section 2, we design the achromatic

#175941 - $15.00 USD Received 11 Sep 2012; revised 28 Oct 2012; accepted 30 Oct 2012; published 18 Mar 2013
(C) 2013 OSA

vector vortex coronagraph by means of Jones calculus and Fourier analysis. We show laboratory demonstrations of the designed achromatic coronagraph in Section 3, and the results in Section 4. In the laboratory demonstrations, we used a photonic-crystal AHP, which has an extremely small central singular point. Finally, we summarize our conclusions in Section 5.

2. Design of an achromatic vector vortex coronagraph

Figure 1 shows an optical configuration of the achromatic vector vortex coronagraph (VVC) using the polarization filtered AHP. In this paper, we assume a circular telescope pupil without shade with a central obscuration and its support structure. The clear circular telescope pupil can be acquired by an off-axis telescope or a subaperture extracted from a conventional on-axis telescope. The VVC and the other focal-plane phase-mask coronagraphs, combined with the clear circular telescope pupil, theoretically enable the perfect rejection of star light as mentioned below. When a telescope pupil has the central obscuration due to a secondary mirror and its support structure, these coronagraphs can not realize the perfect rejection of the star light, and residual star light would prevent us from detecting faint planetary light. We note that, however, several concepts have been proposed for improving the coronagraphic performance with a centrally-obscured telescope [31–33].

The telescope pupil is imaged on an entrance-pupil (EP) plane as shown in Fig. 1(a). The AHP is placed on the focal plane where astronomical targets are imaged by a lens L1. A star light forms a so-called Airy pattern on the focal plane (Fig. 1(b)), when the star is regarded as a point-like light source. An optical vortex with a topological charge $\ell_p = 2$ is embedded on the Airy pattern by the AHP. The AHP is filtered by circular polarizer and analyzer for achromatizing the coronagraphic performance. The circular polarizer and the analyzer are both composed of a polarizer P and a quarter-wave plate QWP (P1 and QWP1 for the circular polarizer, while P2 and QWP2 for the analyzer).

Behind the AHP, the entrance pupil is reimaged by a lens L2, where the on-axis star light is strongly diffracted outside the pupil area as shown in Fig. 1(d). It has been mathematically proved that an intensity of light from a point-like star becomes zero inside the reimaged pupil [5, 6]. A diaphragm called Lyot stop (LS) is placed on the reimaged pupil plane to block the

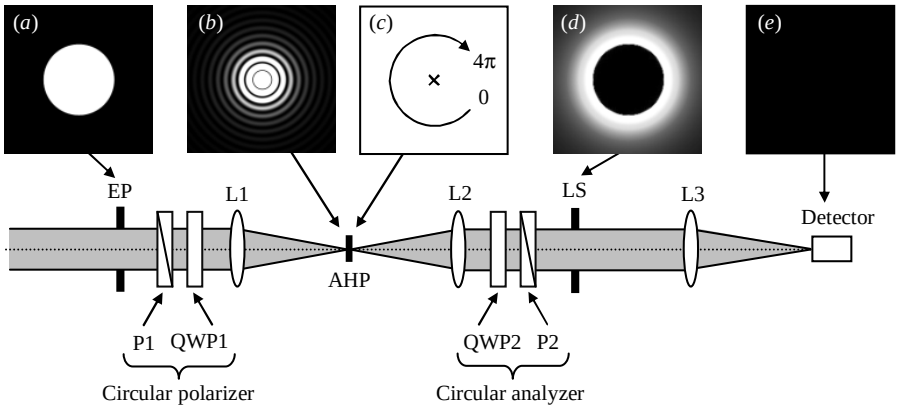


Fig. 1. An optical configuration of the achromatic vector vortex coronagraph. An axially-symmetric half-wave plate (AHP) is placed on a telescope focal plane between circular polarizer and analyzer. The circular polarizer and the analyzer are both composed of a polarizer (P) and a quarter-wave plate (QWP). EP, L, and LS stand for entrance pupil, lens and Lyot stop, respectively.

#175941 - $15.00 USD Received 11 Sep 2012; revised 28 Oct 2012; accepted 30 Oct 2012; published 18 Mar 2013
(C) 2013 OSA

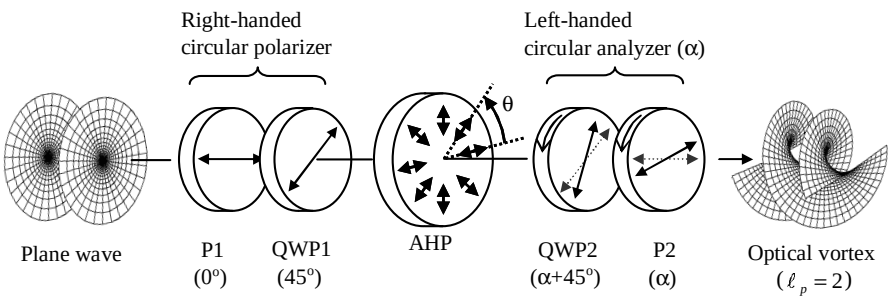


Fig. 2. An optical configuration of the polarization filtered AHP. Lenses in Fig. 1 are not shown here.

Table 1. Summary of axis angles and retardations of the QWP1, AHP, and QWP2.

	QWP1	AHP	QWP2
Axis angles Θ	45°	θ (space variant)	$\alpha + 45^\circ$
Retardations Δ	$90^\circ + \delta_Q$	$180^\circ + \delta_A$	$90^\circ + \delta_Q$

diffracted star light, and to prevent the star light from reaching to a detector on the final focal plane (Fig. 1(e)). On the other hand, faint planets or structures, imaged on an off-center position on the AHP, will be less affected by the coronagraph and reach to the detector. From a point of view of an observational efficiency and an angular resolution, a larger Lyot stop, ideally the same size as the entrance pupil, would be preferable. In laboratory demonstrations described in the following section, we use the Lyot stop 0.9 times smaller than that of the entrance pupil.

Figure 2 shows an optical configuration of the polarization filtered AHP. The circular polarizer generates a right-handed circular polarized light, while the analyzer extracts a left-handed circular one. The circular analyzer can be rotated with respect to the circular polarizer by an angle α.

We investigate the coronagraphic performance as a function of the angle of the circular analyzer α. A state of polarization after the polarizer P1 is described as a Jones vector $\mathbf{E}_i = \begin{bmatrix} 1 \\ 0 \end{bmatrix}$. When the light is passing through the AHP at the azimuth angle θ, an output Jones vector $\mathbf{E}_o$ after the circular analyzer is calculated as

$$\mathbf{E}_o = \mathbf{P}\mathbf{W}_{Q2}\mathbf{W}_A\mathbf{W}_{Q1}\mathbf{E}_i. \tag{1}$$

Here,

$$\mathbf{P} = \begin{bmatrix} \cos^2\alpha & \sin\alpha\cos\alpha \\ \sin\alpha\cos\alpha & \sin^2\alpha \end{bmatrix} \tag{2}$$

is a Jones matrix of the polarizer P2 with an axis α. The three $\mathbf{W}$ matrices ($\mathbf{W}_{Q1}$, $\mathbf{W}_{Q2}$, and $\mathbf{W}_A$) represent the QWP1, QWP2, and AHP, respectively. These optical components are regarded as wave plates, and their Jones matrices are described as

$$\mathbf{W} = \begin{bmatrix} \cos\frac{\Delta}{2} - i\cos 2\Theta \sin\frac{\Delta}{2} & -i\sin 2\Theta\sin\frac{\Delta}{2} \\ -i\sin 2\Theta\sin\frac{\Delta}{2} & \cos\frac{\Delta}{2} + i\cos 2\Theta\sin\frac{\Delta}{2} \end{bmatrix}. \tag{3}$$

The parameters Θ and Δ mean an optic axis and a retardation of the wave plate. We assume that the retardations of the AHP and the QWPs are $\Delta_A = 180^\circ + \delta_A$ and $\Delta_Q = 90^\circ + \delta_Q$, respectively (i.e., δ_A and δ_Q denote retardation errors). Here, the QWPs are assumed to have identical retardations. The axis angles and the retardations assumed here are summarized in Table 1.

#175941 - $15.00 USD Received 11 Sep 2012; revised 28 Oct 2012; accepted 30 Oct 2012; published 18 Mar 2013
(C) 2013 OSA

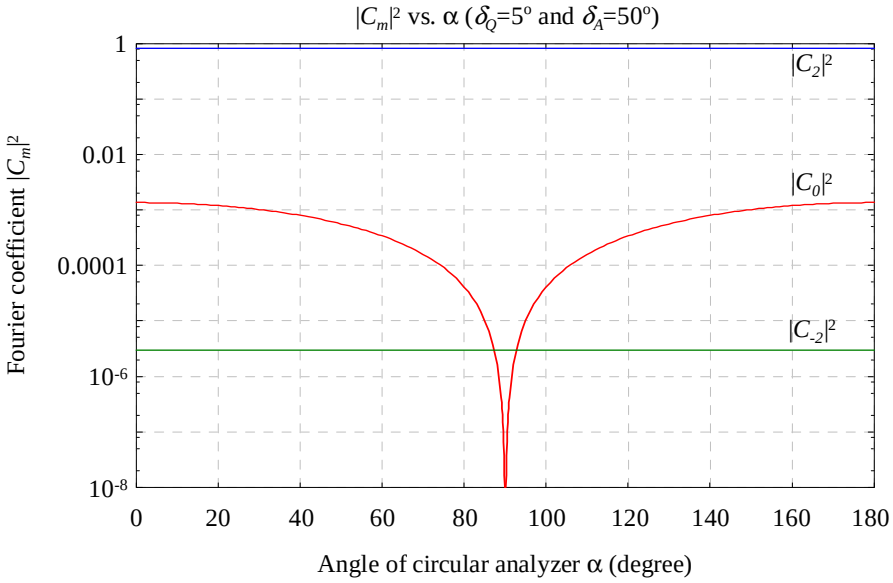


Fig. 3. Fourier coefficients $|C_m|^2$ as a function of an angle of a circular analyzer α, assuming retardation errors $\delta_Q = 5.0^\circ$ and $\delta_A = 50.0^\circ$.

Since the output light from the polarizer P2 is linearly polarized with an angle α, the output vector $\mathbf{E}_o$ can be converted to a vector which has only an x-component by

$$\mathbf{R}\mathbf{E}_o = \begin{bmatrix} \tau \\ 0 \end{bmatrix}. \tag{4}$$

Here, $\mathbf{R}$ is a rotation matrix with an angle of $-\alpha$ as

$$\mathbf{R} = \begin{bmatrix} \cos\alpha & \sin\alpha \\ -\sin\alpha & \cos\alpha \end{bmatrix}. \tag{5}$$

The complex value τ is then regarded as a transmittance (or a mask function) of the polarization filtered AHP, because the input vector $\mathbf{E}_i$ is a unit one. The mask function τ depends on the azimuth angle θ and the retardation errors δ_A and δ_Q.

It is convenient to decompose the mask function into a Fourier series [34]. Each term of the Fourier series represents an ideal optical vortex with an integer topological charge. The mask function is then written as

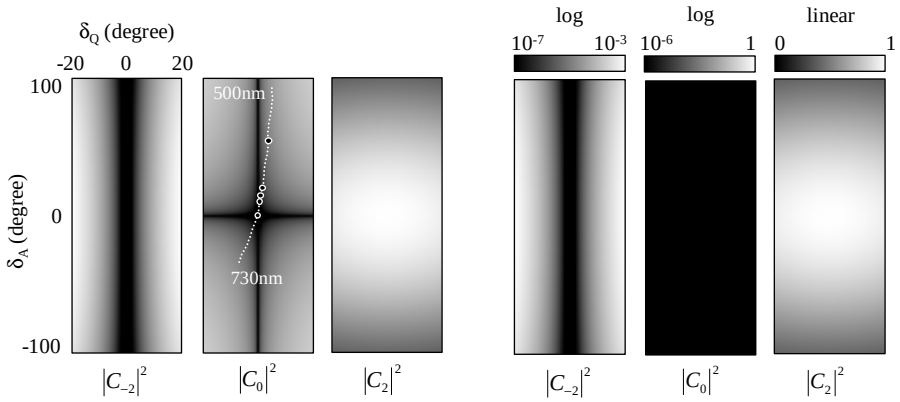
$$\tau(\theta, \delta_A, \delta_Q) = \sum_{m=-\infty}^{\infty} C_m e^{-im\theta}, \tag{6}$$

$$C_m(\delta_A, \delta_Q) = \frac{1}{2\pi}\int_{-\pi}^{\pi} \tau(\theta, \delta_A, \delta_Q) e^{im\theta} d\theta. \tag{7}$$

Here, C_m is a Fourier coefficient of the mth-charged optical vortex.

Figure 3 shows calculated powers of the Fourier coefficients $|C_m|^2$ as a function of the angle of the circular analyzer α. The retardation errors are arbitrarily set to $\delta_Q = 5.0^\circ$ and $\delta_A = 50.0^\circ$. The coefficients only for $m = 0$ and ± 2 become non-zero as shown in the graph, while all the other components ($m = \pm 1, \pm 3, \pm 4, \cdots$) become zero. The result suggests that the component

#175941 - $15.00 USD Received 11 Sep 2012; revised 28 Oct 2012; accepted 30 Oct 2012; published 18 Mar 2013
(C) 2013 OSA



(*a*) α=0º (Non-optimal configuration) (*b*) α=90º (Optimal configuration)

Fig. 4. Fourier coefficients $|C_m|^2$ as a function of retardation errors δ_A and δ_Q, in the case of (a) $\alpha = 0^\circ$ and (b) $\alpha = 90^\circ$. A trajectory of the retardation errors in the laboratory demonstrations is shown in the $|C_0|^2$ map. Five dots on the line correspond to the retardation errors at the five wavelengths of the light source.

of the designed charge $m = 2$ is dominant ($|C_2|^2 \sim 0.82$), while that of $m = -2$ has a small fraction of the power of an order of 10^{-6}. On the other hand, a non-vortex component ($m = 0$) depends on α, and becomes zero at $\alpha = 90^\circ$, while maximum at $\alpha = 0^\circ$.

Figure 3 suggests that the polarization filtered AHP will not become the ideal mask function (i.e., $\tau = e^{-i2\theta}$), when the AHP and the QWPs have the retardation errors. The mask function τ is then written as

$$\tau = C_{-2}e^{i2\theta} + C_0 + C_2 e^{-i2\theta}. \tag{8}$$

In the mask function, both even-charged components $m = \pm 2$ (the first and third terms) theoretically provide perfect stellar rejection for a point-like star [6]. On the other hand, the non-vortex component $m = 0$ (the second term) does not embed any space-variant phase modulation on the stellar image, but reduces the amplitude by a factor of C_0. Thus the effect of this unwanted non-vortex term would appear as a residual Airy pattern on the final focal plane with the reduced intensity $|C_0|^2$. In other words, the value $|C_0|^2$ is directly connected with the coronagraphic performance, that is, a metric of an achievable contrast.

Figure 3 also suggests that the angle of the circular analyzer α must be adjusted accurately to the optimal position ($\alpha = 90^\circ$) to maintain a small value of $|C_0|^2$. For example, the angle α must be adjusted within an accuracy of $\pm 0.16^\circ$ for achieving $|C_0|^2 < 10^{-8}$.

Figure 4 shows the calculated Fourier coefficients $|C_m|^2$ for $m = 0$ and ± 2, in the cases of (*a*) $\alpha = 0^\circ$ and (*b*) $\alpha = 90^\circ$, as a function of the retardation errors δ_Q (between $\pm 20^\circ$) and δ_A (between $\pm 100^\circ$). Again, the other components become zero. The unwanted non-vortex term $|C_0|^2$ becomes zero only for $\delta_Q = 0^\circ$ or $\delta_A = 0^\circ$ when $\alpha = 0^\circ$, while becomes zero for any values of δ_Q and δ_A when $\alpha = 90^\circ$. The results demonstrate that the perfect stellar rejection is realized with the optimal configuration $\alpha = 90^\circ$ even when the AHP and the QWPs are chromatic.

It should be noted that the numerical analyses described in this section assume some idealized conditions. For example, we assume that the polarizers are perfect with infinite extinction ratios, the retardations of two QWPs are identical, and the QWPs and the AHP have perfect transmittances for both polarization states. Numerical analyses for evaluating the coronagraphic performance under realistic conditions will be interesting future works. In Section 4, we will show the effect of the mismatched retardations of the QWPs, in the context of comparison

#175941 - $15.00 USD Received 11 Sep 2012; revised 28 Oct 2012; accepted 30 Oct 2012; published 18 Mar 2013
(C) 2013 OSA

between the numerical analyses and laboratory demonstrations.

3. Laboratory demonstrations

We carried out laboratory demonstrations of the VVC using the AHP manufactured by the photonic-crystal technology [35]. Figure 5 shows a picture, and a microscope image of the photonic-crystal AHP placed between two polarizers (taken by VHX-2000, Keyence Corp.). The AHP was manufactured based on the autocloning technology (the Photonic Lattice, Inc.) [36, 37]. In the microscope image, the polarizers generate a periodic modulation of intensity of transmitted light with the angle θ due to the space-variant fast axes shown in the image. A manufacturing defect at the central phase singularity seems to be extremely small, probably less than 1 μm. We note that a similar photonic-crystal coronagraphic mask, an eight-octant phase mask, has been manufactured based on the same technology [38]. In the microscope image, we can also observe some dark spots, probably due to the measurement process (e.g., nonuniformity of the polarizers).

We constructed the optical setup shown in Fig. 1 to carry out laboratory demonstrations of the VVC. The circular polarizer and the analyzer are placed in the collimated light as shown in Fig. 1. We note that, however, it would be interesting to consider the other configuration, in which the AHP and the polarization filters are all compactly placed on the focal plane. A He-Ne laser with five selectable wavelengths $\lambda = 543$, 594, 604, 612, and 633 nm is used as a model star. The AHP and the QWPs (made of synthetic quartz and MgF_2) have chromatic retardations both optimized at 633 nm. The retardation errors are measured to be $|\delta_Q| < 4^\circ$ and estimated to be $|\delta_A| < 60^\circ$ over the wavelength range of the light source. In Fig. 4(a), we show a trajectory of the retardation errors from $\lambda = 500$ nm (upper right) to 730 nm (lower left) by a white dotted line. Five dots on the line correspond to the retardation errors at the five wavelengths of the light source.

A circular aperture with a diameter of $D = 1.0$ mm is used as an entrance pupil. Focal lengths of the both lenses L1 and L2 are $f = 200$ mm. Thus the size of the Airy disc on the AHP is $2.44\lambda f/D \approx 0.3$ mm, which is much larger than the central phase singularity. A diameter of the Lyot stop is set to be 0.9 mm, that is, 0.9 times smaller than that of the entrance pupil.

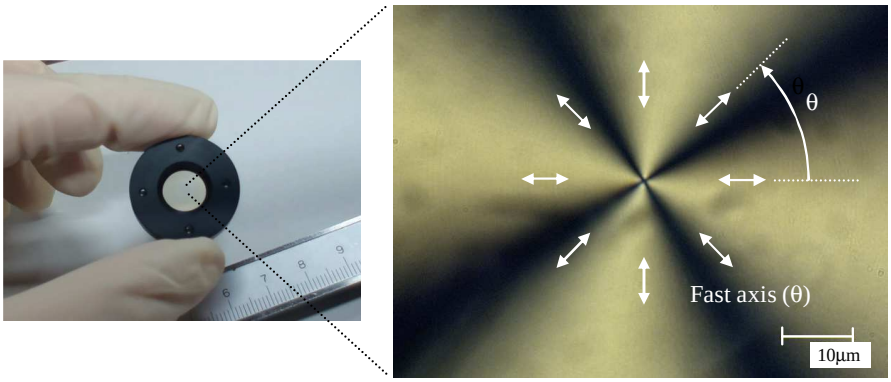


Fig. 5. A picture and a microscope image of a photonic-crystal AHP. The microscope image is taken by placing the AHP between two polarizers.

#175941 - $15.00 USD Received 11 Sep 2012; revised 28 Oct 2012; accepted 30 Oct 2012; published 18 Mar 2013
(C) 2013 OSA

4. Results and discussions

Figure 6 shows the acquired coronagraphic images at the five wavelengths. Intensities of the images are normalized by the peak intensity of the non-coronagraphic image, acquired by displacing the center of the AHP so that the model star is imaged on an off-center position of the AHP. Spots indicated by dotted circles are ghost images. The graph in Fig. 6 shows measured intensity levels averaged over regions within $0.5\,\lambda/D$ from the center (hereafter, I_0). We can see that better achromatic performance is obtained with the optimal configuration $\alpha = 90^\circ$ than the non-optimal one $\alpha = 0^\circ$. The intensity level averaged over the five wavelengths was 3×10^{-4} for $\alpha = 0^\circ$, while improved to 7×10^{-5} for $\alpha = 90^\circ$.

The intensity level at $\lambda = 543$ nm for $\alpha = 0^\circ$ is significantly higher ($I_0 = 1.1 \times 10^{-3}$) than that for $\alpha = 90^\circ$ ($I_0 = 1.9 \times 10^{-4}$). This would be due to the retardation errors δ_Q and δ_A, which are relatively large at $\lambda = 543$ nm (see the trajectory of the retardation errors in Fig. 4(a)), resulting in a substantial unwanted non-vortex term $|C_0|^2$. As mentioned above, the value $|C_0|^2$

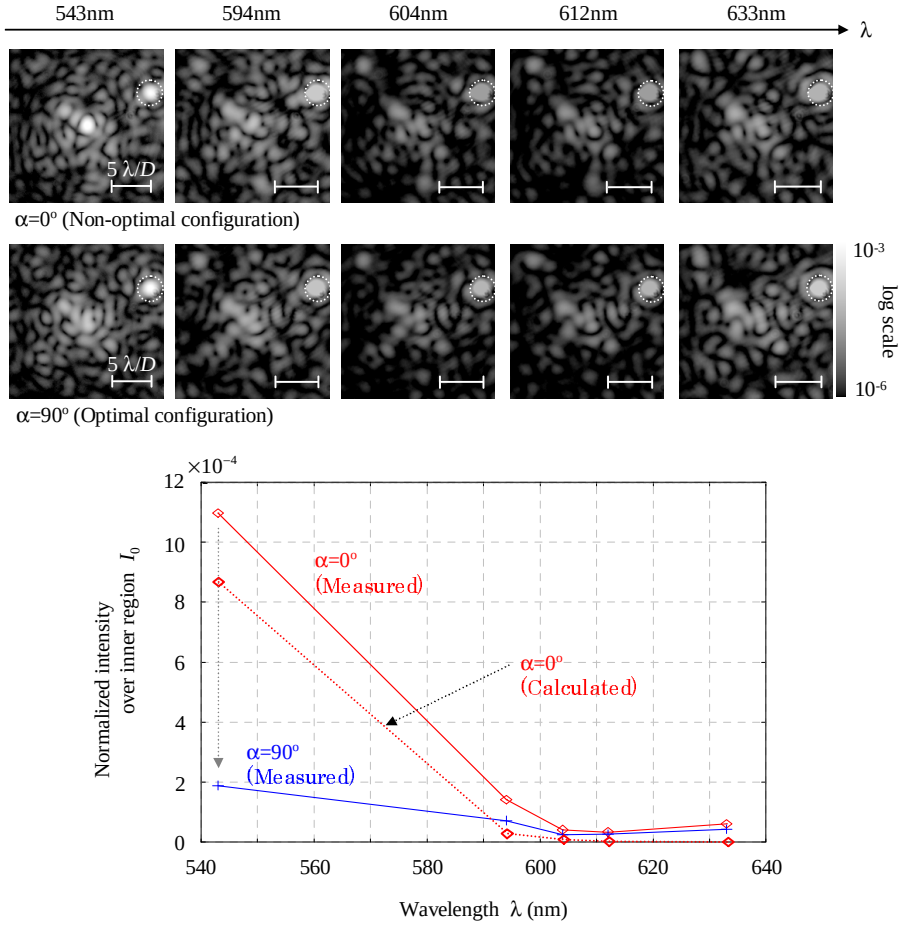


Fig. 6. (*Top*) Coronagraphic images at five wavelengths from $\lambda = 543$ to 633 nm for the non-optimal and optimal configurations ($\alpha = 0^\circ$ and 90°, respectively). (*Bottom*) Intensity levels averaged over regions within $0.5\,\lambda/D$ from the center (I_0), as a function of the wavelength (λ). The dotted line shows calculated I_0 from the results in Fig. 4(a).

#175941 - $15.00 USD Received 11 Sep 2012; revised 28 Oct 2012; accepted 30 Oct 2012; published 18 Mar 2013
(C) 2013 OSA

is connected with the metric of the coronagraphic performance. For example, the metric used here would be written as $I_0 = 0.74|C_0|^2$, where the factor 0.74 comes from the average over the inner regions within $0.5\ \lambda/D$. A dotted line of the graph in Fig. 6 shows the calculated I_0 values derived from the results in Fig. 4(a). The calculated values are consistent with the measured ones.

The acquired coronagraphic images are dominated by residual speckle pattern as shown in Fig. 6. The speckle is probably due to the random phase aberrations of the optical components, even though we used the small entrance pupil with a diameter of 1.0 mm for reducing the phase aberrations of the wavefront incoming to the coronagraph system. We expect that the AHP will less contribute to the residual speckle, since the light passes through the AHP as the Airy pattern with a disc size of ≈ 0.3 mm, while passes through the other components (e.g., the polarizers and the QWPs) as the collimated beam with a size of ≈ 1 mm. For achieving higher contrast, an extreme adaptive optics must be used to clean the wavefront incoming to the coronagraph system.

In Section 2, we assumed that the retardations of the QWPs were identical. We also calculated the Fourier coefficients assuming that the two QWPs have different retardations. The result shows that the difference in the retardations generates the unwanted zero-charged Fourier coefficient C_0 in the mask function τ. Thus, the difference between the retardations of the QWPs must be as small as possible for acquiring the achromatic performance. In our laboratory demonstrations, the difference of the retardations are measured to be about 0.5° at $\lambda = 543$ nm. The value $|C_0|^2$ is then roughly estimated to be 4×10^{-6} (corresponding to $I_0 \approx 3 \times 10^{-6}$), assuming that the retardation errors of the two QWPs are $\delta_{Q1} = 3.75^\circ$, $\delta_{Q2} = 4.25^\circ$ (i.e., $\delta_{Q2} - \delta_{Q1} = 0.5^\circ$) and $\delta_A = 55^\circ$. We expect that this effect cannot be observed in the laboratory demonstrations because the value I_0 is small enough to be buried in the residual speckle.

Figure 2 suggests that the polarizer P1 discards half the incoming light from a target, if it is unpolarized. However, the observational efficiency can be improved by constructing a dual-channel coronagraph by replacing the polarizers with polarization-beam splitters, as proposed in the context of the eight-octant phase-mask coronagraph [38].

5. Conclusion

In this paper, we demonstrated, via the Jones calculus and the Fourier analysis, that the achromatic VVC can be constructed by using the AHP placed between the crossed circular polarizer and the analyzer, even when the chromatic AHP and the QWPs are used. The angle of the circular analyzer has to be set to $\alpha = 90^\circ$ for avoiding the non-vortex term $|C_0|^2$. Our numerical analysis also suggests that the difference in the retardations between two QWPs must be as small as possible to avoid generating the non-vortex term $|C_0|^2$.

We carried out laboratory demonstrations of the VVC over the wavelength from $\lambda = 543$ nm to 633 nm, and compared the performance when the angle of the circular analyzer was set to $\alpha = 0^\circ$ and $\alpha = 90^\circ$. The results exhibit better achromatic performance (the light suppression level of 7×10^{-5}) for the optimal configuration $\alpha = 90^\circ$, as compared to 3×10^{-4} for the non-optimal one $\alpha = 0^\circ$.

Finally, we note that the Jones calculus and the Fourier analysis utilized in this paper will also be convenient for designing achromatic coronagraphs using the other types of phase mask, such as the higher-order vector vortex masks, the four-quadrant and eight-octant phase masks, and so on. The achromatic phase-mask coronagraph will become a powerful tool for removing bright star light over broad wavelength range, and enable us to characterize extremely faint planetary light through spectroscopic observations.

#175941 - $15.00 USD Received 11 Sep 2012; revised 28 Oct 2012; accepted 30 Oct 2012; published 18 Mar 2013
(C) 2013 OSA

Acknowledgments

We are grateful to Takayuki Kawashima of the Photonic Lattice Inc. for useful information on a photonic-crystal device. This research was partially supported by the National Astronomical Observatory of Japan (NAOJ), and the Japan Society for the Promotion of Science (JSPS) through KAKENHI (21340041, 23740139).

#175941 - $15.00 USD Received 11 Sep 2012; revised 28 Oct 2012; accepted 30 Oct 2012; published 18 Mar 2013
(C) 2013 OSA